equilibria. For example, in contrast to the results presented above for increases in Ga concentration, increases in the Al concentration achieved by adding pure Al wire to aluminosilicate solutions leads to a depolymerization of oligomeric anions.[27-29] The dissolution of 1 mol of pure Al consumes 1 mol of hydroxide ions to produce 1 mol of aluminate anions, but the addition of 1 mol of Ga^{3+} ions consumes 4 mol of hydroxide ions to produce 1 mol of gallate anions. Thus, the addition of $Ga(NO_3)_3$ to silicate solutions causes a greater reduction in the pH of the solution than the addition of pure Al. The lower pH results in an increase in the extent of solution polymerization. It is also noted by ^{29}Si NMR peak widths that the exchange rates between gallate anions and small silicate anions (i.e., dimer and linear trimer anions) is faster than those observed for aluminosilicate solutions. Faster exchange rates result in broad ^{29}Si NMR peaks which are indistinguishable from the background noise. Finally, Ga prefers to incorporate into silicate anions where the SiO–Ga–OSi bond angle is rather acute, i.e., in S3R(1Ga) and D3R(1Ga) anions, due to the larger size of Ga atoms compared to Al or Si atoms. On the other hand, Al incorporates into a wide variety of silicate anions. The overall size of the anion might limit the stabilization of gallosilicate anions larger than the D3R(1Ga) or D4R anions due to the effect of cation crowding.[48] This explains why D4R(1Ga) and doubly Ga substituted anions are not observed. The smaller size of Al allows for stabilization of significant concentrations of D4R(1Al) anions and aluminosilicate anions exhibiting $Q_3(2Al)$, $Q_2(2Al)$, and $Q_{3\Delta}(2Al)$ connectivities.

Conclusions

The present investigation demonstrates the usefulness of ^{29}Si and ^{71}Ga NMR spectroscopies for studying tetralkylammonium gallosilicate solutions. Gallosilicate anions with Si atoms of $Q_{2\Delta}(1Ga)$, $Q_2(1Ga)$, and $Q_{3\Delta}(1Ga)$ connectivities are observed in TPA gallosilicate solutions. Specific ^{29}Si NMR resonances assigned to Si atoms in S3R(1Ga), b-S3R(1Ga), and D3R(1Ga) anions were identified. S3R(1Ga) anions are especially stable and become the dominant species as the solution temperature is raised to near synthesis conditions. Ga atoms undergo a fast chemical exchange with the dimer and linear trimer silicate anions, causing the ^{29}Si peaks for Si atoms in dimer(1Ga) and linear trimer(1Ga) anions to broaden into the background noise. ^{71}Ga NMR experiments provide evidence for the chemical exchange of Ga atoms between gallate anions and gallosilicate anions, but ^{71}Ga NMR spectra cannot generally be resolved to give peaks for Ga atoms associated with specific siloxane bond connectivities. Only at silicate ratios of greater than 2 can ^{71}Ga spectra be resolved into two peaks, one for gallate anions and one for Ga atoms in gallosilicate oligomers. A simple set of chemical equilibria explains the changes in the distribution of solution species with changes in the SiO_2, Ga, and TPA_2O concentrations. Gallate anions appear to react preferentially with low molecular weight silicate anions (i.e., dimer and linear trimers) compared to the case of higher molecular weight silicate anions. Substitution of 50 vol % water by DMSO in TPA gallosilicate solutions forces all of the dissolved Si into S3R, S3R(1Ga), b-S3R, b-S3R(1Ga), D3R, D3R(1Ga), and D4R anions. No ^{29}Si resonances for D4R(1Ga) anions are observed. Although ^{71}Ga NMR experiments of TMA gallosilicate solutions display peaks assigned to Ga atoms in gallosilicate anions, ^{29}Si NMR experiments provide no evidence for solution oligomers with Ga–O–Si bonds. The larger size of GaO_4^{5-} tetrahedra compared to SiO_4^{4-} tetrahedra may prohibit the formation of anions the size of D4R(1Ga) anions in tetraalkylammonium gallosilicate solutions, in contrast to what is observed for reactions between aluminate and silicate anions.

Acknowledgment. This work was supported by the Director, Office of Energy Research, Office of Basic Energy Sciences, Materials Sciences Division of the U.S. Department of Energy, under Contract DE-AC03-76SF00098, and by a grant from W. R. Grace and Co. Fellowship support for R. F. Mortlock was provided by Upjohn Co.

Registry No. Ga, 7440-55-3.

Electronic Structure of Retinal and Related Polyenals in the Lowest Triplet State: An Electron Spin Echo Study

Marianne Ros, Marcel A. Hogenboom, Peter Kok, and Edgar J. J. Groenen*

Centre for the Study of Excited States of Molecules, Huygens Laboratory, University of Leiden, P.O. Box 9504, 2300 RA Leiden, The Netherlands *(Received: September 20, 1991)*

We have observed transitions between the spin sublevels of the lowest triplet state T_0 of the all-trans isomers of retinal and methyl-substituted polyenals by means of electron spin echo spectroscopy in a magnetic field and in zero field. This triplet state appears to be $\pi\pi^*$ in nature. The frequencies of the zero-field transitions have been determined. For retinal we have observed the T_z–T_x transition at 2370 MHz and the T_z–T_y transition at 1990 MHz. The upper spin sublevel T_z dominates the populating of T_0 and decays fastest, but the selectivity in the decay is clearly less than in the populating. The lifetimes of the individual sublevels of the lowest triplet state of retinal are 71 μs for T_x, 17 μs for T_y, and 12 μs for T_z at 1.2 K. The data for retinal correspond to those for a linear polyenal with six double bonds. This shows that the carbon–carbon double bond in the cyclohexene ring of retinal is also involved in the excitation, which suggests that the chromophoric part of retinal is approximately planar in the lowest triplet state.

1. Introduction

Light absorption by the retinal chromophore of rhodopsin and bacteriorhodopsin represents the first step in two biological processes that have been actively explored on a molecular scale in recent years. Photoexcitation causes isomerization of this chromophore and thereby initiates a sequence of chemical reactions eventually enabling vision and bacterial photosynthesis. To elucidate the underlying mechanisms, a detailed knowledge of the electronically excited states of retinal is required. The chromophore of retinal is a conjugated carbon chain ending in an aldehyde group (see Figure 1).

It is well established nowadays that for polyenes longer than butadiene the lowest excited singlet state is of A_g character, and consequently the optical transition from S_0 to this state is electric-dipole forbidden.[1] The transition seen in absorption corre-

(1) (a) Hudson, B. S.; Kohler, B. E. *Chem. Phys. Lett.* **1972**, *14*, 299. (b) Schulten, K.; Karplus, M. *Chem. Phys. Lett.* **1972**, *14*, 305.

0022-3654/92/2096-2975$03.00/0

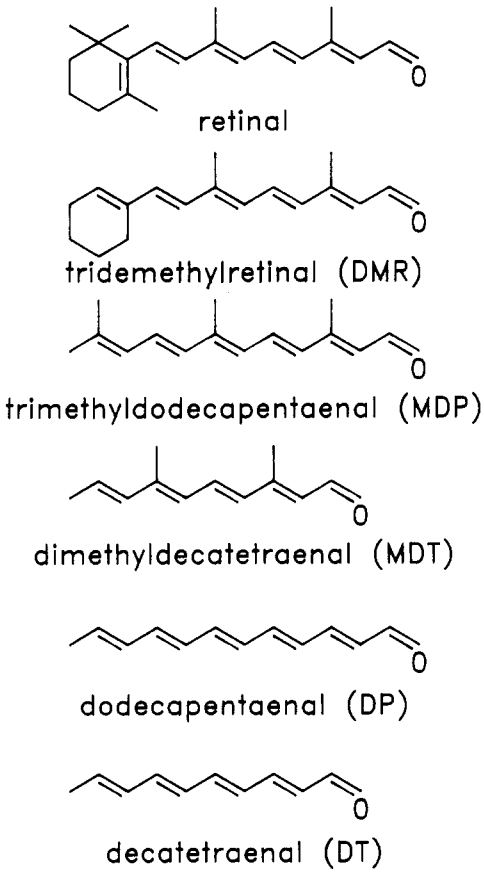

Figure 1. Molecular structure of the compounds presently investigated and of dodecapentaenal and decatetraenal.

sponds to the excitation of one electron from the highest occupied to the lowest unoccupied molecular orbital resulting in a singlet state of B_u character. The presence of the carbonyl bond in retinal removes the inversion symmetry and adds $n\pi^*$ excited states. The group of Becker[2] undertook an elaborate study of absorption and emission spectral properties of retinal and some homologues, differing in the number of carbon–carbon double bonds, in order to determine the singlet-state ordering for these compounds. From the dependence of the fluorescence quantum yield on environmental conditions they inferred that the lowest excited singlet state of a free retinal molecule is of $n\pi^*$ character, while for a hydrogen-bonded retinal molecule it is of $\pi\pi^*$ character and the analogue of the polyene A_g state.

A study of the lowest triplet state of retinal is severely hampered by the absence of phosphorescence. Raubach and Guzzo[3] concluded from singlet–triplet absorption spectra recorded in the presence of high-pressure oxygen that the triplet state lies about 12450 cm^{-1} above S_0. From triplet–triplet absorption spectra at room temperature the quantum yield of intersystem crossing was found to be 0.6 ± 0.1[4] and the lifetime of T_0 to be 9 μs.[5] A clear reduction of the C=C stretch frequency upon triplet excitation, observed in time-resolved resonance Raman studies,[6] seems to indicate that in the lowest triplet state the bond order of the C=C bonds is reduced. Up to now, knowledge about the electronic nature of T_0 has been lacking.

Here we present a study of the lowest triplet state of *all-trans*-retinal by electron spin echo spectroscopy. In a recent investigation of all-trans polyenals, e.g., dodecapentaenal and decatetraenal (see Figure 1), we have concluded the lowest triplet state for these compounds to be of $\pi\pi^*$ character and we have determined the relative energies and the rates of populating and decay of the spin sublevels.[7,8] In view of the equal number of double bonds for dodecapentaenal and retinal one would expect their triplet states to be similar. However, steric hindrance between the cyclohexene ring and the polyenal chain may well lead to a nonplanar structure for retinal. For the ground state this has indeed been found; X-ray studies point to a skewed 6-s-cis structure with a dihedral angle of approximately 60° between the planes of the cyclohexene ring and the polyenal chain.[9] On the other hand, semiempirical calculations suggest that the C_6–C_7 torsional angle decreases upon singlet $\pi\pi^*$ excitation.[10] A skewed C_6–C_7 conformation for retinal may to some extent decouple the sixth double bond, which is incorporated in the cyclohexene ring, from the rest of the π-electron system. We therefore include not only dodecapentaenal but also decatetraenal for comparison. In addition, we consider various methyl-(de)substituted analogues (see Figure 1) in order to bridge the gap between polyenals and retinal. In doing so, we attempt to assign the differences between the triplet states of these compounds—if any—to the influence of either the methyl substituents along the chain or the cyclohexene ring.

We report the observation by electron spin echo spectroscopy of transitions between the triplet spin sublevels for the all-trans isomers of retinal, trimethyldodecapentaenal, dimethyldecatetraenal, and tridemethylretinal (Figure 1) dissolved in polyethylene. For the former three compounds we have deduced the fine-structure tensor and the populating ratios and decay rates of the individual spin states. The lowest triplet of retinal is found to be a $\pi\pi^*$ state, and this is also the case for the other compounds under study. Comparison of the data unequivocally bears out the resemblance between the triplet state of retinal, that of dodecapentaenal, and that of trimethyldodecapentaenal. The electronic structure of the lowest triplet state of retinal equals that of a polyenal containing six double bonds, which demonstrates that in the triplet state the double bond in the cyclohexene ring is part of the π-electron system. Both the methyl groups along the chain and the cyclohexene ring only slightly affect the zero-field splittings and the relative populating rates of the triplet state as compared to that of the unsubstituted polyenals, whereas these substituents, in particular the methyl groups, significantly modify the decay rates.

2. Materials and Methods

all-trans-Retinal (retinal, 95%) was purchased from Aldrich and *all-trans*-1,1′,5-tridemethylretinal (DMR) was supplied by the group of Lugtenburg. *all-trans*-3,7,11-Trimethyl-2,4,6,8,10-dodecapentaenal (MDP) and *all-trans*-3,7-dimethyl-2,4,6,8-decatetraenal (MDT) were synthesized from shorter aldehydes via a Horner–Emmons condensation with diethyl (3-carbonitrilo-2-methyl-2-propenyl)phosphonate followed by a reduction with diisobutylaluminum hydride.[11] Cis and trans isomers of the methyl-substituted polyenals were separated by column chromatography (column, Merck silica gel 60, 230–240 mesh; eluent, 20/80 vol % ether/petroleum ether). All compounds were identified by their 200-MHz ^1H NMR spectra and electronic absorption spectra. Even when stored as a solution in a hydrocarbon solvent, they still deteriorate at −20 °C under a nitrogen atmosphere in the dark. Consequently, prior to use they were purified by HPLC. All molecules presently investigated are found to be unstable upon optical excitation with ultraviolet light at 1.2 K.

Polyethylene films, made from linear low-density polyethylene pellets (Wacker Chemie), were stretched by approximately 500%.

(2) (a) Das, P. K.; Becker, R. S. *J. Phys. Chem.* **1978**, *82*, 2081. (b) Das, P. K.; Becker, R. S. *J. Phys. Chem.* **1978**, *82*, 2093. (c) Takemura, T.; Das, P. K.; Hug, G.; Becker, R. S. *J. Am. Chem. Soc.* **1978**, *100*, 2627.
(3) Rauback, R. A.; Guzzo, A. V. *J. Phys. Chem.* **1971**, *75*, 983.
(4) Bensasson, R.; Land, E. J.; Truscott, T. G. *Photochem. Photobiol.* **1973**, *17*, 53.
(5) Truscott, T. G.; Land, E. J.; Sykes, A. *Photochem. Photobiol.* **1973**, *17*, 43.
(6) (a) Wilbrandt, R.; Jensen, N.-H. *J. Am. Chem. Soc.* **1981**, *103*, 1036. (b) Wilbrandt, R.; Jensen, N.-H. *Ber. Bunsen-Ges. Phys. Chem.* **1981**, *85*, 508.
(7) Ros, M.; Groenen, E. J. J. *Chem. Phys. Lett.* **1989**, *154*, 29.
(8) Ros, M.; Groenen, E. J. J. *J. Chem. Phys.* **1991**, *94*, 7640.
(9) Hamanaka, T.; Mitsui, T.; Ashida, T.; Kakudo, M. *Acta Crystallogr. B* **1972**, *28*, 214.
(10) Warshel, A.; Karplus, M. *J. Am. Chem. Soc.* **1974**, *96*, 5677.
(11) Muradin-Szweykowska, M.; Pardoen, J. A.; Dobbelstein, D.; Van Amsterdam, L. J. P.; Lugtenburg, J. *Eur. J. Biochem.* **1984**, *140*, 173.

The methyl-substituted polyenals were embedded in the film after stretching, by soaking the films in a saturated *n*-pentane (Merck p.A.) solution at room temperature. Because for retinal a sufficiently concentrated sample could not be prepared in this way, this compound was dissolved in the polyethylene film before stretching. For the zero-field experiments we employed unstretched films, since we noticed that the degree of alignment did not influence the observations.

All compounds were optically excited at 355 nm by the third harmonic of a Quanta Ray DCR-2 Nd:Yag laser, which operated at 10 Hz. To avoid photoselection, the laser beam was depolarized by passing it through a quartz rod. The samples were illuminated with about 5 mJ/pulse.

The electron spin echo (ESE) experiments were performed at 1.2 K by applying a two-pulse echo sequence at a time t_d after the laser flash, the $\pi/2$ and π pulses being separated by a time τ. The homodyne X-band spectrometer was identical to that employed in ref 8. We applied a prepulse before the laser flash in order to suppress a background echo at $g = 2$. The heterodyne 2–4 GHz zero-field spectrometer has been described in ref 12. The heterodyne 1–2 GHz zero-field instrumentation was similar to its 2–4-GHz counterpart, except for the minimum time interval τ between the two microwave pulses, which amounted to 1500 and 1200 ns, respectively. In all spectrometers we employed $\pi/2$ pulses with a typical duration of 200 ns.

The phase memory time T_2, defined as $I_{echo}(\tau) \propto e^{-2\tau/T_2}$ was measured in X-band for retinal, MDT, and MDP. The decay patterns were modulated by the interaction between the electron spin and the nuclear spins and showed a slight dependence on the orientation of $\vec{B}_0$. On the average we found the following values of T_2: 2.0 ± 0.3 μs for retinal, 2.0 ± 0.2 μs for MDT, and 1.8 ± 0.2 μs for MDP. For DP we previously found a slightly larger value of 3.2 ± 0.4 μs for T_2.[8]

The ESE-detected EPR spectra were recorded by monitoring the echo intensity as a function of the strength of the magnetic field. These spectra were simulated according to a model developed by Kottis and Lefèbvre for triplet EPR spectra,[13] which we extended to allow for the description of transient EPR spectra of partially oriented samples.[8] We define $\vec{l}$ as the direction within a molecule that is parallel to the stretch direction $\vec{s}$ of the film in case the molecule is perfectly aligned, and we describe the orientation distribution of the molecules in the film with a Gaussian:

$$f(\beta) \propto e^{-\beta^2/\omega^2}$$

where β represents the angle between $\vec{l}$ and $\vec{s}$. By optimizing the correspondence between the simulated and the experimental spectra, we deduced the values of the zero-field parameters X, Y, and Z, the line width λ of the EPR transition, and the width ω of the orientation-distribution function (see section 3). The populating ratios used for calculating the spectra were obtained from the decay curves. These relative populating rates could not be retrieved from the simulations because the relative intensities of the different bands in the experimental and simulated spectra could not be compared with each other. This originates from the use of the ESE technique in recording the EPR spectra, which leads to distortions of the experimental spectra.[14] First, distortions of the spectra result from the τ dependence of the modulations on the decay curve. The modulation pattern depends on $\vec{B}_0$ and accordingly the shape of the EPR spectra varies with τ as well. This effect decreases in importance on increasing the magnitude of $\vec{B}_0$. As a consequence the high-field parts of the spectra are least deformed. Second, optimization of the pulsing conditions for a certain band in the spectrum may distort or reduce the echo signal at other values of the magnetic field. We could minimize the distortion of the EPR spectra by applying $\pi/2$ pulses of 200 ns. Moreover, the more random the distribution of the molecules, the more pronounced the distortion. For highly anisotropic samples such as those of the unsubstituted polyenals the narrow distribution function dominates the line shape. The simulation procedure itself also contains an approximation that hampers a quantitative comparison of experimental and simulated spectra. This concerns the assumption that the orientation-distribution function depends only on the angle β between $\vec{l}$ and $\vec{s}$ and that all orientations of the molecule that mutually differ in the angle γ, which represents rotation about the molecular $\vec{l}$ axis, are equally probable. This approximation is justified only for disklike or rodlike molecules such as the unsubstituted polyenals or for a sharp distribution in β. By calculating EPR spectra for several discrete values of γ, we inferred that the neglect of the γ dependence does not essentially affect the interpretation of the experimental EPR spectra.

3. Results

Upon pulsed laser excitation into the singlet manifold, we have observed X-band ESE signals for retinal, MDP, and MDT. We have recorded EPR spectra, which vary with the orientation of the magnetic field $\vec{B}_0$ with respect to the anisotropic sample in a way expected for spectra that derive from a triplet state. The spectra depend only on the orientation of $\vec{B}_0$ with respect to the stretch direction. The sample shows cylindrical symmetry, and consequently a study of the spectra as a function of magnetic-field orientation can be restricted to one plane containing $\vec{s}$. We took this plane to be the plane of the polyethylene film. In Figure 2a we display the ESE-detected EPR spectra observed for retinal at different orientations of $\vec{B}_0$. They cover a range of 0.2 T and show approximately mirror symmetry with respect to $g = 2$ except for a sign change; all low-field signals are emissive (E) and all high-field signals are absorptive (A). In a search for the canonical orientations, we have observed that for $\angle(\vec{B}_0,\vec{s}) = 90 \pm 2°$ (upper spectrum of Figure 2a) the resonance fields corresponding to those peaks in the spectrum that are marked with an asterisk become stationary with respect to small variations in the direction of the magnetic field. The fields corresponding to maximum emission and absorption in the lower spectrum of Figure 2a hardly vary with the orientation of $\vec{B}_0$ in the range $0° < \angle(\vec{B}_0,\vec{s}) < 20°$. Consequently, the canonical orientation of $\vec{B}_0$ related to the marked peaks in this spectrum must be in this range but cannot be accurately determined. A third canonical orientation, which is to be expected since we deal with a triplet state, has not been distinguished. The structure of the retinal spectra can more easily be grasped when we first discuss the spectra for the methyl-substituted polyenals MDP and MDT.

For MDP and MDT we find three canonical orientations of $\vec{B}_0$ in the plane of the film. For MDP these directions make angles of 90 ± 2°, 74 ± 4°, and 16 ± 2° with $\vec{s}$, for MDT of 90 ± 2°, 73 ± 5°, and 18 ± 2°. Henceforth, we denote these directions with $\vec{X}$, $\vec{Y}$, and $\vec{Z}$, respectively. In Figure 3 we display the EPR spectra of MDP for $\vec{B}_0 \parallel \vec{X}$, $\vec{B}_0 \parallel \vec{Y}$, and $\vec{B}_0 \parallel \vec{Z}$. These spectra resemble those previously obtained for the unsubstituted polyenals.[8] Methyl substitution makes the features at the stationary resonance fields less pronounced, but one can distinguish between these relatively sharp peaks, in Figure 3 indicated by asterisks, and broad shoulders. A qualitative explanation of the EPR spectra therefore proceeds along similar lines as for DP.[7,8] The origin of the spectral shape lies in the uniaxial distribution of the molecules in the film. Misaligned molecules yield a broadening of the peaks at the stationary resonance fields. The less aligned the sample, the less pronounced these peaks. The broad wings are due to well-aligned molecules whose principal axes of the fine-structure tensor are not parallel to $\vec{B}_0$. The shoulder in Figure 3 for $\vec{B}_0 \parallel \vec{Y}$, for instance, can be understood as originating from molecules that yield the stationary lines for $\vec{B}_0 \parallel \vec{X}$. Upon changing the direction of the magnetic field from $\vec{B}_0 \parallel \vec{X}$ to $\vec{B}_0 \parallel \vec{Y}$, these lines develop into broad bands and their resonance fields are no longer stationary. As previously, we can reason that $\vec{X}$, $\vec{Y}$, and $\vec{Z}$ correspond to the principal axes of the fine-structure tensor of one triplet state, although the observed canonical orientations are not mutually perpendicular; these directions are related to molecules that occupy different positions in the polyethylene film according to the

(12) Van't Hoff, C. A. Ph.D. Thesis, University of Leiden, 1977.
(13) Kottis, P.; Lefèbvre, R. *J. Chem. Phys.* **1963**, *39*, 393.
(14) Mims, W. In *Electron Paramagnetic Resonance*; Geschwind, S., Ed.; Plenum Press: New York, 1972; Chapter 4, p 263.

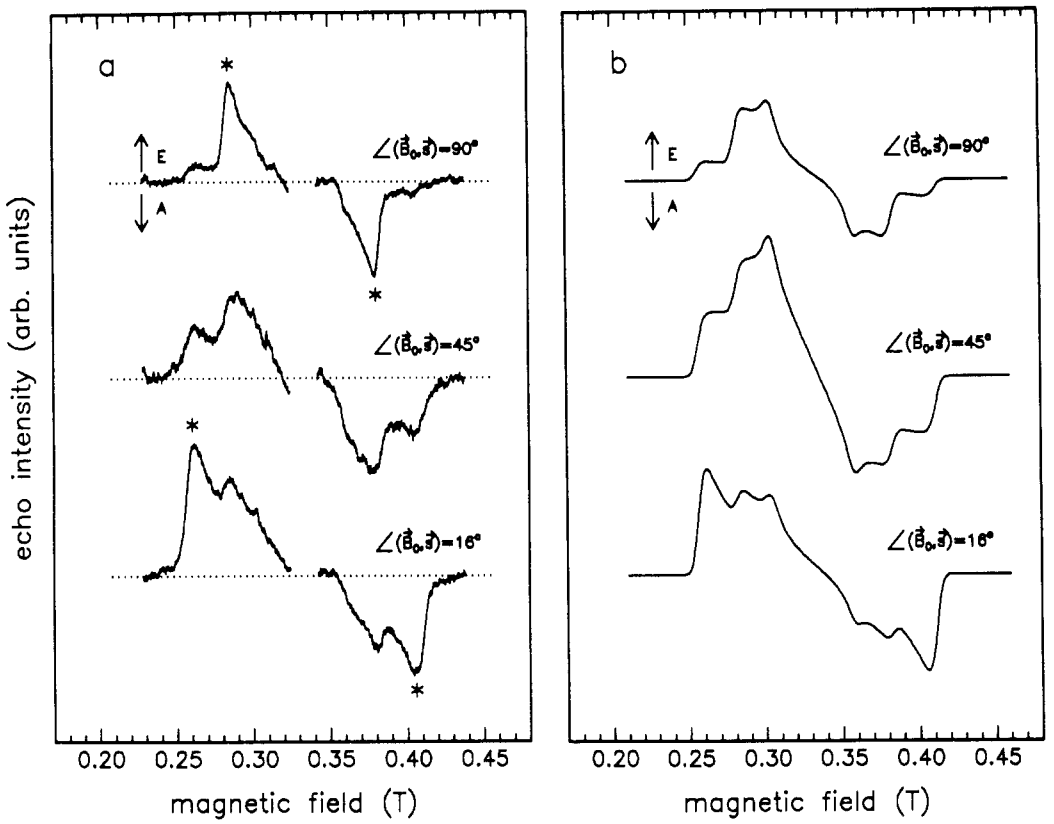

Figure 2. (a) ESE-detected EPR spectra of retinal in a stretched polyethylene film for several orientations of $\vec{B}_0$ with respect to $\vec{s}$. The resonance fields of the peaks marked with an asterisk are stationary with regard to small variations in the direction of the magnetic field. The dotted baselines only serve as a guide to the eye. The high- and low-field parts of the spectra have been recorded separately. The relative intensities of the spectra for different orientations are arbitrary. E denotes emission and A absorption of microwaves. The microwave frequency is 9356 MHz, t_d is 300 ns, and τ is 500 ns. (b) Numerical simulations of the ESE-detected EPR spectra of retinal for several orientations of $\vec{B}_0$ with respect to $\vec{s}$. The relative populating rates employed are those given in Table III, the angle between $\vec{l}$ and $\vec{z}$ is taken to be 16°. The zero-field parameters, the line width λ, and the distribution width ω have been optimized in order to obtain the best agreement between experimental and simulated spectra (Table I). The simulated spectra correspond to a superposition of calculated spectra for aligned molecules and for randomly oriented molecules in the ratio 40/60 (cf. Figure 4). The intensities of the simulated spectra are mutually comparable.

cylindrical symmetry. With this explanation for the ESE-detected EPR spectra of the methyl-substituted polyenals in mind, we return to the spectra of retinal.

The two canonical orientations found for retinal, by analogy with MDP and MDT denoted as $\vec{X}$ (upper spectrum in Figure 2a) and $\vec{Z}$ (lower spectrum in Figure 2a), refer to the directions of the principal axes of the fine-structure tensor of retinal's lowest triplet state. For $\vec{B}_0 \parallel \vec{X}$ we notice that the main features look almost identical to those of MDP, but that next to those marked peaks additional shoulders are visible at the outer parts of the spectrum. For $\vec{B}_0 \parallel \vec{Z}$ the peaks corresponding to the stationary resonance fields become slightly broader upon addition of the cyclohexene ring. Unlike for MDP the wings are not smooth; broad, structured sidebands arise. On closer inspection it turns out that for retinal at each orientation of the magnetic field features corresponding to bands in the $\vec{B}_0 \parallel \vec{X}$ and $\vec{B}_0 \parallel \vec{Z}$ spectra of MDP are present; the orientation dependence merely consists of a variation of the relative intensities of the different parts in the spectrum. This is illustrated by the intermediate spectrum in Figure 2a ($\angle(\vec{B}_0,\vec{s}) = 45°$), in which we observe how the different bands develop in passing from one extreme ($\vec{B}_0 \parallel \vec{X}$) to another ($\vec{B}_0 \parallel \vec{Z}$). An understanding of this phenomenon and of its relation to the anisotropy of the retinal sample has been acquired from a simulation of the EPR spectra.

We have performed numerical simulations of the ESE-detected EPR spectra for retinal, MDP, and MDT. For the methyl-substituted polyenals and retinal the angle between $\vec{l}$ and the principal $\vec{z}$ axis, required to carry out the calculations, has been taken equal to 16° (see section 4). For all compounds the relative populating rates have been obtained from the decay curves (vide infra). Several parameters have been varied in the simulations until the correspondence between calculated and experimental spectra was optimal. In this way we have determined the zero-field parameters from the stationary resonance fields for $\vec{B}_0 \parallel \vec{X}$ and $\vec{B}_0 \parallel \vec{Z}$, the line width λ from the steepness of the accompanying onsets, and the distribution width ω from the width of the peaks corresponding to the stationary resonance fields (Table I). For MDP and MDT the experimental spectra are well reproduced. Comparison of the parameters obtained for these compounds with those of DP demonstrates that upon methyl substitution (DP → MDP, DT → MDT) both λ and ω increase. Shortening of the polyenal (MDP → MDT, DP → DT) causes an increment of λ, but hardly of ω. The parameters λ and ω, as deduced from the spectra according to the above criteria, increase considerably on adding the cyclohexene ring (MDP → retinal). Simulations with these large values of the parameters, however, do by no means reproduce the experimental spectra of retinal. Especially the observation that variation of the direction of $\vec{B}_0$ only leads to a change in the relative intensities of different parts in the spectrum does not follow from such simulations. Agreement between experimental and simulated spectra is acquired if we assume a certain fraction of the retinal molecules to be not aligned at all but to be randomly oriented. This is illustrated in Figure 4. The upper spectrum

TABLE I: Simulation Parameters for Retinal, MDP, and MDT That Were Optimized To Obtain Agreement between Experimental and Simulated EPR Spectra. Parameters for DP and DT[8] Added for Comparison

	λ, G	ω, rad	X/h, MHz	Y/h, MHz	Z/h, MHz
retinal	60 ± 5	0.45 ± 0.05	−940 ± 10	−500 ± 10	1440 ± 10
MDP	25 ± 3	0.20 ± 0.02	−916 ± 5	−538 ± 5	1454 ± 5
MDT	40 ± 5	0.20 ± 0.02	−1104 ± 10	−674 ± 10	1778 ± 10
DP	20 ± 3	0.13 ± 0.02	−956 ± 5	−584 ± 5	1540 ± 5
DT	30 ± 3	0.15 ± 0.02	−1154 ± 5	−733 ± 5	1887 ± 5

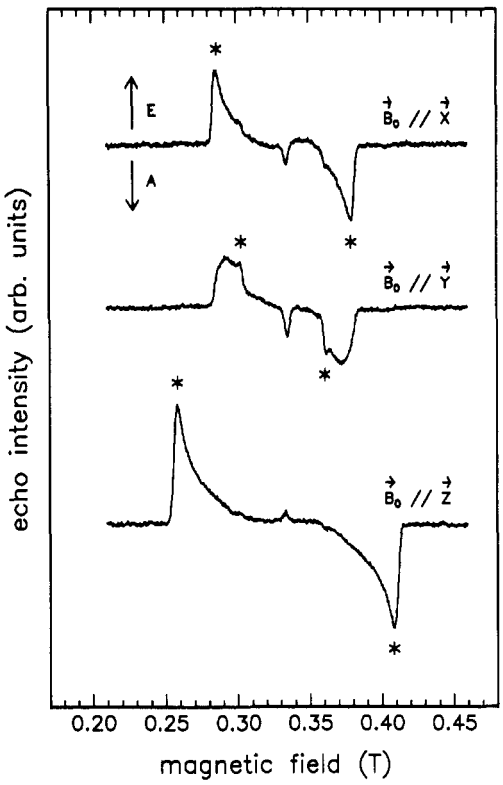

Figure 3. ESE-detected EPR spectra of trimethyldodecapentaenal in a stretched polyethylene film for $\vec{B}_0$ parallel to $\vec{X}$, $\vec{Y}$, and $\vec{Z}$. The resonance fields of the peaks marked with an asterisk are stationary with regard to small variations in the direction of the magnetic field. The microwave frequency is 9356 MHz, t_d is 300 ns, and τ is 500 ns.

in this figure represents a simulation of an aligned sample of retinal for $\angle(\vec{B}_0,\vec{s}) = 16°$ and a value of $\omega = 0.45$ rad (cf. Table I). Although this simulation reproduces the width of the marked peaks in the lower spectrum of Figure 2a, which correspond to the stationary resonance fields for $\vec{B}_0 \parallel \vec{Z}$, the broad, structured sidebands are absent in the simulated spectra. Figure 4b represents a simulation of a random sample of retinal. Addition of simulated spectra for an aligned and for a random sample in the ratio 40/60 yields the spectrum in Figure 4c, which shows all the features present in the experimental spectrum for $\vec{B}_0 \parallel \vec{Z}$ in Figure 2a. Employing this model, i.e., assuming the sample to consist of 40% aligned and 60% randomly oriented molecules, we could simulate the experimental spectra for the other orientations of $\vec{B}_0$ rather satisfactorily as well (Figure 2b). As can be seen from comparing the spectra in Figure 2a with those in Figure 2b the relative intensities still do not match well. In particular, the magnitude of the most central features, corresponding to those peaks that we expect to be stationary for $\vec{B}_0 \parallel \vec{Y}$, is different in experimental and calculated spectra. As mentioned before, we ascribe this discrepancy mainly to distortions in the experimental spectra, which arise because they are recorded by using the ESE technique.

We have observed the T_z–T_x and T_z–T_y transitions in zero field for retinal, DMR, MDP, and MDT. In Table II we enumerate the frequencies and widths of the zero-field transitions as obtained from these experiments. The signal-to-noise ratio of the retinal and DMR echoes was about one-third of that for MDP and one-tenth of that for the echoes detected for DP previously. Since for retinal the T_z–T_y transition is at the border of the frequency ranges of the 1–2- and 2–4-GHz ESE spectrometers, the signal-to-noise ratio of this echo was even smaller. Consequently, the value for the corresponding frequency is less accurate and the width of the transition could not be determined at all. We observed for retinal the T_z–T_x transition at 2370 MHz and the T_z–T_y transition at 1990 MHz. These frequencies agree with those derived from the simulation of the EPR spectra (Table I) within experimental accuracy. The absolute values of the zero-field parameters are derived from the EEE/AAA pattern of the EPR spectra in combination with the relative populating rates of the

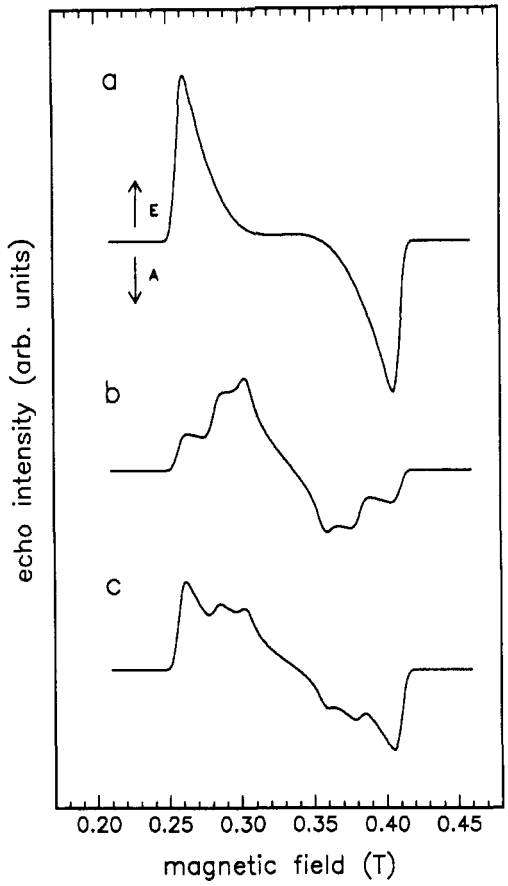

Figure 4. Numerical simulations of the ESE-detected EPR spectra of retinal. The relative populating rates employed are those given in Table III. The angle between $\vec{l}$ and $\vec{z}$ is taken to be 16°. The values used for the zero-field parameters, the line width λ, and the distribution width ω are given in Table I. (a) Sample of aligned molecules ($\omega = 0.45$ rad) for $\angle(\vec{B}_0,\vec{s}) = 16°$. (b) Sample of randomly oriented molecules ($\omega = 1000$ rad). (c) Superposition of the simulations of Figure 4, parts a and b, in the ratio 40/60.

TABLE II: Frequencies of the Zero-Field Transitions of Retinal, DMR, MDP, and MDT As Determined from ESE Experiments in Zero Field[a]

	$(Z-X)/h$, MHz	fwhm, MHz	$(Z-Y)/h$, MHz	fwhm, MHz
retinal	2370 ± 15	135 ± 20	1990 ± 40	
DMR	2435 ± 15	100 ± 15	2055 ± 10	50 ± 10
MDP	2360 ± 10	80 ± 10	1995 ± 10	50 ± 10
MDT	2870 ± 15	100 ± 10	2460 ± 10	100 ± 10
DP	2496 ± 3	24 ± 3	2125 ± 3	23 ± 3
DT	3041 ± 4	31 ± 3	2620 ± 3	29 ± 3

[a] The sublevel ordering has been obtained from the EEE/AAA pattern in the EPR spectra in combination with the relative populating rates. The values for DP and DT[8] have been added for comparison.

triplet spin sublevels (vide infra). From a transient EPR study Rösch reported for retinal in a liquid crystal the T_z–T_x and T_z–T_y transitions to be at 2179 and 1969 MHz,[15] frequencies that are somewhat lower than those obtained here for retinal in polyethylene.

We have investigated the populating and decay of the triplet spin sublevels for retinal, MDP, and MDT both in zero field and in a magnetic field by monitoring the echo intensity as a function of t_d, the delay of the microwave pulse sequence with respect to the laser flash. The echo decay reflects the time development of the population difference of the two spin sublevels connected:

$$I_{echo}(t_d) = p_1 e^{-k_1 t_d} - p_2 e^{-k_2 t_d} \quad (1)$$

(15) Rösch, N. Ph.D. Thesis, University of Stuttgart, 1989.

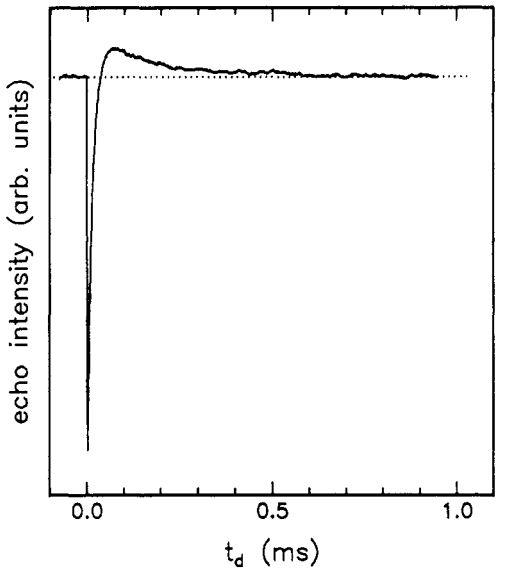

Figure 5. Echo intensity for retinal as a function of the delay time t_d between the laser flash and the first microwave pulse: high-field transition for $\vec{B}_0 \parallel \vec{X}$ with τ = 500 ns, $|\vec{B}_0|$ = 0.38 T.

TABLE III: Relative Populating Rates for the Spin Sublevels of T_0 for Retinal, MDP, and MDT[a]

	p_x	p_y	p_z
retinal	0.043 ± 0.010	0.080 ± 0.040	0.877 ± 0.035
MDP	0.045 ± 0.010	0.110 ± 0.050	0.845 ± 0.040
MDT	0.023 ± 0.010	0.039 ± 0.020	0.938 ± 0.020
DP	0.030 ± 0.010	0.060 ± 0.015	0.910 ± 0.020
DT	0.030 ± 0.010	0.045 ± 0.010	0.925 ± 0.010

[a] The values for p_x are the average of those obtained in zero-field and X-band experiments (see text). The values for DP and DT[8] have been added for comparison.

A typical example of a decay curve is displayed in Figure 5. All curves show sign inversion with p_1 about an order of magnitude larger than p_2. Consequently, in case k_1 is also substantially larger than k_2, we can better determine k_2 by applying a population–inversion pulse at a fixed time just after the laser flash and varying the delay of the monitoring pulse sequence with respect to this inversion pulse. Precise determination of the dynamic properties is hampered by some experimental complications, which we described in detail in a previous paper.[8] Moreover, the EPR spectra for retinal are less well resolved than those for the polyenals; for example, for $\vec{B}_0 \parallel \vec{X}$ the marked peaks corresponding to stationary resonance fields are superposed on the tail of the outermost features (Figure 2a). Populating and decay rates have been determined as follows: We acquire k_z from the decay of the high-field echo corresponding to the marked peaks for $\vec{B}_0 \parallel \vec{Z}$. By monitoring the evolution of the marked peaks at high magnetic field for $\vec{B}_0 \parallel \vec{X}$, we obtain a value for the fast decay constant k_1, which in the high-field approximation equals $^1/_2(k_y + k_z)$. By combining this k_1 with k_z, we derive k_y. Employing the population-inversion method, we retrieve the rate constant k_x from the T_z–T_x transition in zero field and from the high-field $\vec{B}_0 \parallel \vec{X}$ transition in a magnetic field. The relative populating rates are obtained from the preexponential factors of the decay curves for the high-field $\vec{B}_0 \parallel \vec{X}$ and $\vec{B}_0 \parallel \vec{Z}$ transitions. In Tables III and IV we summarize the relative populating rates and the decay rates for the triplet spin sublevels.

4. Discussion

The results described in the preceding section enable us to identify the electronic structure of the lowest triplet state of retinal. Consideration of the observed triplet sublevel ordering, zero-field splittings, and dynamic properties prove that the lowest triplet state of retinal (and that of the methyl-substituted polyenals) is $\pi\pi^*$ in nature. In the present section we will elaborate the arguments that lead to this assignment and discuss the properties

TABLE IV: Decay Rates for the Spin Sublevels of T_0 for Retinal, MDP, and MDT[a]

	k_x, ms^{-1}	k_y, ms^{-1}	k_z, ms^{-1}	k_x/k_z	k_y/k_z
retinal	14.0 ± 2.5	59 ± 12	85 ± 4	0.16 ± 0.04	0.70 ± 0.20
MDP	12.0 ± 1.5	53 ± 13	95 ± 7	0.13 ± 0.03	0.55 ± 0.20
MDT	6.5 ± 1.5	34 ± 7	55 ± 2	0.12 ± 0.03	0.62 ± 0.17
DP	4.6 ± 0.5	25 ± 4	73 ± 5	0.063 ± 0.010	0.34 ± 0.07
DT	1.9 ± 0.2	8 ± 1	36 ± 3	0.053 ± 0.010	0.22 ± 0.05

[a] The values for k_x are the average of those obtained in zero-field and X-band experiments (see text). The values for DP and DT [8] have been added for comparison.

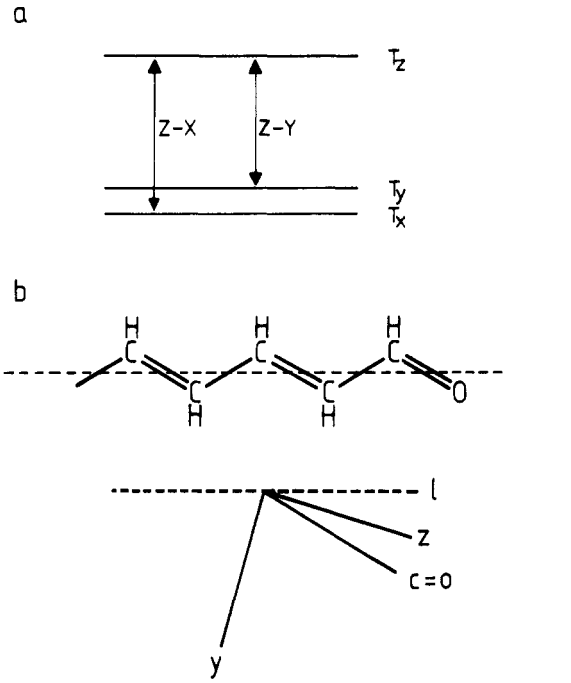

Figure 6. (a) Spin sublevel ordering of the $^3\pi\pi^*$ state for the all-trans isomers of retinal and the polyenals. (b) Position of the $\vec{y}$ and $\vec{z}$ principal axes of the fine-structure tensor with respect to the polyenal chain. The $\vec{x}$ axis is perpendicular to the chain.

of the $^3\pi\pi^*$ state for these compounds in relation to that for the unsubstituted polyenals. In particular, we focus on the influence of the substituents on the electronic structure and the populating and decay, on the question whether the π-bond in the cyclohexene ring is part of the conjugated electron system, and on the C_6–C_7 single-bond conformation. Besides, we will discuss the orientation of the retinal molecules in the stretched polyethylene film.

The spin sublevel ordering for retinal and the methyl-substituted polyenals in T_0 is displayed in Figure 6a; T_z is the upper spin sublevel and T_y and T_x invariably are close in energy ($\Delta E \approx 400$ MHz). This is the same scheme as found for the $^3\pi\pi^*$ state of the unsubstituted polyenals.[8]

The frequencies of the zero-field transitions observed for retinal, DMR, MDP, and DP are all in the same range (Table II). The frequency corresponding to the T_z–T_x transition shows a maximum variation of only 6%; for retinal and MDP these values are even nearly identical. On the other hand, for DT and MDT this transition is found at a frequency approximately 20% higher than that for retinal. Apparently, the model compounds for retinal are MDP and DP, and not MDT and DT. The electronic structure of the lowest triplet state of retinal corresponds to that of a polyenal with a total number of six double bonds. This indicates that the carbon–carbon double bond of retinal that is part of the cyclohexene ring fully participates in the triplet excitation. Previously we have concluded that DP is a planar molecule in the lowest triplet state.[8] The close correspondence observed between the zero-field splittings of DP and those of retinal suggests that the chromophoric part of the latter molecule is more or less planar as well. Unfortunately, the lack of any quantitative data on the variation of the zero-field splittings for small C_6–C_7 torsional angles

precludes a more precise conclusion. We recall that X-ray data for single crystals[9] and calculations for retinal and a retinal analogue[16,17] indicate that retinal in the ground state has a skewed 6-s-cis conformation with a dihedral angle of 50–60°. If this is the case for retinal in a polyethylene film as well, our results point to a profound geometry change toward a much more planar structure upon triplet excitation. Such a geometry change has also been predicted by Warshel and Karplus for the singlet $\pi\pi^*$ excitation.[10] These authors calculated the C_6–C_7 torsional angle to be smaller in the $^1\pi\pi^*$ state than in the ground state. In this context we note that time-resolved resonance Raman experiments on retinal indicate that in the lowest triplet state the bond order of the C=C bonds becomes smaller and that of the C—C bonds becomes larger.[6] If this would apply to the C_6—C_7 bond, the enhanced double-bond character could well bring the adjacent parts of the retinal molecule in a more planar conformation.

From the above it is obvious that neither the chain methyl groups nor the cyclohexene ring exert a profound influence on the triplet electronic structure. Nevertheless, small variations in the zero-field frequencies do occur upon substitution along the polyenal backbone. Apart from these slight frequency shifts the presence of substituents causes significant inhomogeneous broadening of the zero-field transitions. This broadening already occurs upon methyl substitution along the chain and becomes even larger when the cyclohexene ring is added (cf. Table II). The broader lines for the substituted molecules may well reflect a wider distribution of conformations due to differences in methyl-group orientations and in torsional angles of carbon–carbon single bonds, in particular of the C_6—C_7 bond for retinal.

Unlike unsubstituted polyenals it is not obvious from the molecular shape how retinal and the methyl-substituted polyenals are preferentially aligned in the stretched film. However, the direction of $\vec{l}$ in these molecules can be derived from the following arguments: First, from the similarity of the electronic structure of the lowest triplet state, we expect the principal axes of the fine-structure tensor for DP, MDP, and retinal to have approximately the same direction within the molecular frame. Second, we have learned that the canonical orientations for MDP and retinal are approximately identical to those for DP. The observed angles between $\vec{s}$ and the canonical orientations equal the angles between $\vec{l}$ and the principal axes, because we defined $\vec{l}$ to be the direction that is parallel to $\vec{s}$ for a perfectly aligned molecule. Since for the rodlike unsubstituted polyenals we argued that $\vec{l}$ is parallel to the polyene chain,[8] we infer that for MDP and retinal $\vec{l}$ is parallel to the polyenal chain as well. This conclusion is supported by the simulations of the EPR spectra for these compounds. If we take $\vec{l}$ parallel to the chain, the experimental spectra are well reproduced. The presently determined direction of $\vec{l}$ contradicts the conclusion of Margulies et al.[18] On the basis of the low dichroic ratio observed for retinal absorption spectra in stretched polyethylene film, they argued that retinal will be oriented "with the plane of the ring parallel to the stretching direction of the film, the long polyene chain being displaced from that direction". In Figure 6b we display the directions of $\vec{l}$, $\vec{y}$, and $\vec{z}$ with respect to the polyenal chain as derived from our experiments for the all-trans isomers of retinal and the polyenals. The principal axis $\vec{x}$ is perpendicular to the plane of the chromophore.

The presence of the substituents does not markedly affect the populating process. The relative populating rates of the triplet spin sublevels of retinal and MDP are within the experimental accuracy equal to those of DP, which corroborates the similarity of T_0 of these compounds. Characteristic is that p_z is about an order of magnitude larger than both p_y and p_x. The relative populating rates of retinal and the methyl-substituted polyenals can be explained with the same simple model as adopted for the unsubstituted polyenals.[8] Intersystem crossing is determined by first-order spin–orbit coupling between the $^1n\pi^*$ state and the lowest $^3\pi\pi^*$ state. The dominant contribution arises from the local interaction on the oxygen atom. On intersystem crossing a spin state is prepared that is a linear combination of T_y and T_z with the spin aligned in the plane perpendicular to the carbonyl bond. If the $\vec{z}$ axis would be parallel to this C=O bond, p_z would equal 1; the small nonzero value of p_y is explained by the small angle (±14°) between the directions of the $\vec{z}$ axis and the C=O bond. The populating rate p_x vanishes entirely only if the compound under study is strictly planar in the excited states and if higher-order spin–orbit coupling is negligible.

Unlike for the zero-field parameters and the relative populating rates, addition of substituents on the polyenal chain significantly influences the radiationless decay of T_0. As shown in Table IV, the lifetimes of all sublevels become shorter and the sublevel selectivity decreases. The change already occurs upon methyl substitution, while the presence of the cyclohexene ring does not noticeably affect the decay anymore. The decay rates of the individual sublevels for retinal are virtually identical to the corresponding ones for MDP, which substantiates the close similarity of their triplet states.

The average rate constant k_{av} of both retinal and MDP at 1.2 K corresponds to a lifetime $\tau = k_{av}^{-1}$ of 19 μs, which is about twice as large as the value observed for retinal at room temperature.[5] The small temperature dependence of the radiationless decay indicates that it concerns an intramolecular process, as we previously assumed it to be for the unsubstituted polyenals. For the latter compounds of different chain length we found the decay rates to decrease exponentially with increasing T_0–S_0 energy gap, which points to the dominant role that Franck–Condon factors play in the decay process. The lifetime τ for DP at 1.2 K amounts to 30 μs,[8] somewhat larger than for retinal. We note that this difference can not be traced back simply to an increment in the Franck–Condon factors. On the one hand, the T_0–S_0 energy gap was found to be larger for retinal than for DP (12 450 cm^{-1} (ref 3) as compared to 11 050 cm^{-1} (ref 19)), which would point to smaller Franck–Condon factors and so to a slower decay for retinal. On the other hand, the relative number of C–H accepting modes increases upon methyl substitution, which may point to larger Franck–Condon factors and so to a faster decay for retinal.

Anyhow, the increment of the decay rates upon methyl substitution cannot solely arise from an increase in the Franck–Condon factors, since this would influence the decay of all spin sublevels to the same extent. Evidently this is not the case; both k_x and k_y increase more than k_z (see Table IV). This decrease in selectivity must have its origin in the electronic matrix elements. However, the interpretation of the sublevel selectivity in such terms is less clear-cut for the decay than for the populating of T_0. There is no dominant first-order spin–orbit coupling term that governs the decay from T_0 to the ground state S_0. Several second-order terms involving vibronic and spin–orbit interactions play a role. Consequently, the selectivity in the decay may be much less than in the populating process, which we indeed observed for the unsubstituted polyenals.[8] Upon methyl substitution the selectivity diminishes further and k_y even becomes about equal to k_z. We expect this to be mainly related to a change in vibronic-coupling terms upon addition of substituents, because the methyl groups may well perturb the skeletal modes of the polyenal chain. Vibrational analysis of retinal in the electronic ground state has shown that upon methyl substitution the C–C stretches are not delocalized along the chain anymore, since there is a strong coupling of in-plane methyl rocks and C–CH_3 stretches with adjacent C–C stretches.[20]

A spinoff of the present investigations concerns the incorporation of retinal molecules in stretched polyethylene films. The present experiments have shown that the retinal molecules preferentially align their polyenal chain along the stretch direction of the polyethylene film. As already mentioned, this is incompatible with

(16) Rowan, R.; Warshel, A.; Sykes, A.; Karplus, M. *Biochemistry* **1974**, *13*, 970.
(17) Poirier, R. A.; Yadav, A. *Chem. Phys. Lett.* **1989**, *156*, 122.
(18) Margulies, L.; Friedman, N.; Sheves, M.; Mazur, Y.; Lippitsch, M. E.; Riegler, M.; Aussenegg, F. R. *Tetrahedron* **1985**, *41*, 191.
(19) Evans, D. F. *J. Chem. Soc.* **1960**, 1735.
(20) Curry, B.; Broek, A.; Lugtenburg, J.; Mathies, R. *J. Am. Chem. Soc.* **1982**, *104*, 5274.

Margulies' conclusion,[18] based on the low dichroic ratio (d_0 = 1.8) observed for retinal in stretched polyethylene film, that the cyclohexene ring will be parallel to $\vec{s}$. In addition, we have concluded from the simulations that the ESE-detected EPR spectra of retinal cannot be reproduced by taking one value for the distribution width ω. The retinal molecules are dispersed among two (or more) fractions that are aligned to a different degree. At least one of these fractions shows a more or less random distribution. This conclusion enables us to understand the origin of the low dichroic ratio observed for retinal in a stretched film; we simulated EPR spectra for retinal with a model in which 40% of the molecules are aligned according to a Gaussian function with a width of 0.45 rad and 60% of the molecules are randomly oriented. Such a distribution would yield a dichroic ratio of 1.6, to be compared with the value of 1.8 reported for a similar sample by Margulies et al.[18] The distribution of the retinal molecules among several fractions provides for a plausible explanation of the low dichroic ratio and accordingly corroborates the conclusion that $\vec{l}$ is parallel to the chain. From EPR spectra observed for anthracene in stretched polyethylene film, Phillips et al. also suggested that the solute molecules are dispersed among an oriented and an unoriented fraction.[21] They relate this to dielectric relaxation studies, which indicate that such fractions may be located in regions of different polymer arrangement.[22]

(21) Brown, I. M.; Phillips, P. J.; Parikh, D. *Chem. Phys. Lett.* **1986**, *132*, 273.
(22) Yang, Y. T.; Phillips, P. J.; Thulstrup, E. W. *Chem. Phys. Lett.* **1982**, *93*, 66.

5. Conclusion

Electron spin echo spectroscopy has enabled us to identify the electronic structure of the nonradiative lowest triplet state of *all-trans*-retinal. We have found this triplet state to be of $\pi\pi^*$ character. Its fine-structure tensor, relative populating rates and decay rates, can be described in similar terms as for the polyenals that lack the cyclohexene ring. From the strong resemblance between the present results and those for a polyenal containing six double bonds, we infer that the cyclohexene double bond in retinal fully participates in the triplet excitation. This conclusion leads to the suggestion that the part of the retinal molecule that contains the π-electron system is planar in T_0.

Concerning the influence of the substituents we have noticed that in comparison with the unsubstituted polyenals the presence of the chain methyl groups slightly affects the zero-field parameters and to a larger extent the decay rates. On the other hand, both zero-field parameters and decay rates remain strikingly the same on going from trimethyldodecapentaenal to retinal. From these observations we deduce that the presence of the cyclohexene ring modifies the electronic structure of T_0 less than addition of the methyl groups at the chain.

Acknowledgment. We are grateful to Professor J. Lugtenburg for supplying us with DMR and for his continuous interest in this research project. We thank Jan Coremans for his assistance in recording the ESE-detected EPR spectra. This work was supported by the Netherlands Foundation for Chemical Research (SON) with financial aid from the Netherlands Organization for Scientific Research (NWO).

Resonantly Enhanced Multiphoton Ionization of N_2 $a''^1\Sigma_g^+$ ($v' = v''$) ← $X^1\Sigma_g^+$ ($v'' = 0, 1, 2$). 2. Alignment and Orientation Measurements

Thomas F. Hanisco, Chun Yan, and Andrew C. Kummel*

Department of Chemistry, University of California, San Diego, La Jolla, California 92093
(Received: September 20, 1991; In Final Form: December 3, 1991)

The N_2 $a''^1\Sigma_g^+ \leftarrow X^1\Sigma_g^+$ (0,0) 2 + 1 resonance-enhanced multiphoton ionization (REMPI) transition has been used to measure angular momentum alignment and orientation of N_2 scattered from Ag(111). This two-photon $\Sigma \leftarrow \Sigma$ transition has been used for the first time to measure angular momentum alignment and orientation moments. Alignment of N_2 molecules has been measured using the O, Q, and S branches, and orientation has been measured using the O and S branches. For the alignment measurements employing excitation of the Q branch by linearly polarized light, the effects of optical ellipticity and polarization saturation have been investigated as well as the sensitivity of the calculated alignment to our estimate of the character of the virtual state in the N_2 $a''^1\Sigma_g^+ \leftarrow X^1\Sigma_g^+$ (0,0) transition. For the orientation measurements, two different techniques were employed and compared. In the first technique, the optical ellipticity is varied while the major axis of polarization is fixed in space. In the second technique, the optical ellipticity and the direction of the major axis of ellipticity are simultaneously varied. The S and O branches are highly sensitive to alignment and orientation, yielding excellent values for $A_{0+}^{[2]}$ and $A_{1-}^{[1]}$ but less accurate values for $A_{0+}^{[4]}$ and $A_{1-}^{[3]}$. The Q branch, though less sensitive than the O and S branches, yields good qualitative values for the $A_{0+}^{[2]}$ alignment moment in the limit of very small optical ellipticity and near-zero saturation.

I. Introduction

This paper is concerned with the theoretical and experimental determination of angular momentum alignment and orientation in Σ-Σ two-photon absorption. Angular momentum alignment refers to an anisotropic distribution of magnetic sublevels, M, in which there is preferential population of sublevels with a given absolute magnitude, $|M|$. For diatomic molecules, alignment results in the molecules having a preference for cartwheeling vs helicoptering rotational motion. Angular momentum orientation refers to an anisotropic distribution of magnetic sublevels in which positive M versus negative M sublevels are preferentially populated. For diatomic molecules, angular momentum orientation results from the propensity of the molecules to rotate in a clockwise versus counterclockwise direction. Mathematically, angular momentum orientation describes an anisotropic distribution of positive versus negative M sublevels. To quantify angular momentum polarization, the distribution of M sublevels is described by the moments of the polarization distribution, $A_{q\pm}^{[k]}$. The moments with odd values of index k quantify the orientation while the moments with even values of index k quantify the angular momentum alignment. This paper describes the measurements of absorption probability versus optical polarizations and the calculational techniques required to determine these polarization moments $A_{q\pm}^{[k]}$ for the special case of a Σ-Σ two-photon absorption. The Σ-Σ two-photon absorption is unusual because it is dominated by a strong Q branch which is a poor probe of angular momentum polarization, but this Q

0022-3654/92/2096-2982$03.00/0